

# Time-Resolved Self-Assembly of a Fullerene-Topology Core–Shell Cluster Containing 68 Uranyl Polyhedra

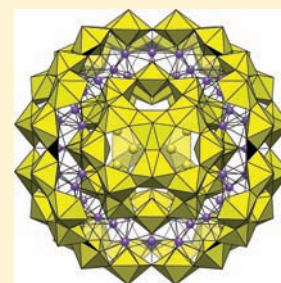
Jie Qiu,<sup>†</sup> Jie Ling,<sup>†</sup> Audrey Sui,<sup>†</sup> Jennifer E. S. Szymanowski,<sup>†</sup> Antonio Simonetti,<sup>†</sup> and Peter C. Burns<sup>\*,†,‡</sup>

<sup>†</sup>Department of Civil Engineering and Geological Sciences, University of Notre Dame, Notre Dame, Indiana 46556, United States

<sup>‡</sup>Department of Chemistry and Biochemistry, University of Notre Dame, Notre Dame, Indiana 46556, United States

**S** Supporting Information

**ABSTRACT:** A complex core–shell cluster consisting of 68 uranyl peroxo polyhedra, 16 nitrate groups, and  $\sim 44$   $K^+$  and  $Na^+$  cations was obtained by self-assembly in alkaline aqueous solution under ambient conditions. Crystals formed after a month and were characterized. The cluster, designated as  $\{U_1C_{28}CU_{40R}\}$ , contains a fullerene-topology cage built from 28 uranyl polyhedra. A ring consisting of 40 uranyl polyhedra linked into five-membered rings and 16 nitrate groups surrounds this cage cluster. Topological pentagons in the cage and ring are aligned, and their corresponding rings of uranyl bipyramids are linked through  $K^+$  cations located between the two shells. A partially occupied U site is located at the center of the cluster. Time-resolved small-angle X-ray scattering and electrospray ionization mass spectrometry demonstrated that the  $U_{28}$  cage cluster formed in solution within an hour, whereas the  $U_{40R}$  shell formed around the cage cluster after more than several days.



## 1. INTRODUCTION

Polyoxometalate clusters based on transition metals are structurally diverse and offer broad applications.<sup>1–6</sup> These are usually synthesized in one-pot reactions and form through the condensation of metal–oxygen polyhedra into various building units that further self-assemble. The details of these self-assembly mechanisms remain generally poorly understood.<sup>7</sup> Whereas transition-metal-based polyoxometalates have been studied for decades, researchers have only recently begun to focus on the self-assembly of complex actinide oxide clusters. The lighter actinides present a wealth of accessible oxidation states and rich coordination chemistry,<sup>8</sup> suggesting they may form clusters that rival the complexity and diversity known for transition metals. Over the past few years, actinide-based clusters have emerged as a fertile area of research. The self-assembly of U(IV) and U(V) oxide clusters have been reported by Nocton,<sup>9–11</sup> Biswas,<sup>12</sup> and Duval.<sup>13</sup> Soderholm<sup>14</sup> presented the structure of a Pu(IV) oxide cluster with the fluorite-type structure. We have reported a series of more than 30 U(VI) uranyl-based cage clusters that self-assemble in aqueous solution under ambient conditions.<sup>4,15–26</sup> In these clusters, uranyl ions are bridged by peroxo ligands that are bidentate to the uranyl ions, and this inherently bent  $U-O_2-U$  unit<sup>27,28</sup> fosters the formation of cages with curved walls. Many of these clusters contain bridges between uranyl ions other than peroxo, including hydroxyl, oxalate, methylenediphosphonate, and pyrophosphate groups.

We are interested in the continued development of actinide-based polyoxometalates because of their potential applications in an advanced nuclear fuel cycle, among other reasons. For example, cage clusters built from uranyl polyhedra can have masses that exceed 20 kDa and diameters of  $\sim 3$  nm, suggesting the possibility of separation of uranium contained in such cage

clusters from complex solutions solely on the basis of their size or mass. Cage clusters of uranyl polyhedra also contain cavities and pores of various sizes, presenting the possibility of conducting chemical reactions in confined environments, as suggested for various transition-metal polyoxometalates.

Only rarely have polyoxometalates been observed to form core–shell clusters.<sup>7,29</sup> None of the reported cage clusters built from uranyl polyhedra involve a core–shell configuration, and little information is available concerning the mechanisms or rates of uranyl cluster formation. Here we report the synthesis and characterization of a core–shell cluster built from uranyl polyhedra and nitrate ions, designated as  $\{U_1C_{28}CU_{40R}\}$ , and studies of its self-assembly as a function of time using small-angle X-ray scattering (SAXS) and electrospray ionization mass spectrometry (ESI-MS).

## 2. EXPERIMENTAL METHODS

**2.1. Synthesis of  $\{U_1C_{28}CU_{40R}\}$ .** *Caution:* Although depleted uranium was used in these experiments, it is radioactive and should only be handled by qualified personnel in appropriate facilities.

Crystals containing the  $\{U_1C_{28}CU_{40R}\}$  cluster were initially synthesized by loading aqueous solutions of  $UO_2(NO_3)_2 \cdot 6H_2O$  (0.5 M, 0.1 mL),  $H_2O_2$  (30%, 0.1 mL), tetraethylammonium hydroxide (40%, 0.1 mL), malonic acid (0.5 M, 0.1 mL), NaCl (0.5 M, 0.125 mL), and KCl (0.5 M, 0.125 mL) into a 5 mL glass vial. The resulting solution was clear with a pH of 11.2. Yellow block-shaped crystals formed after about 1 month when the solution was left standing in contact with air under ambient conditions. The yield of crystals was  $\sim 16\%$  on the basis of uranium. This synthesis was repeated three times, and each run gave  $\sim 3.1$  mg of crystals. The synthesis was scaled up by a factor of 10, and the quantity of crystals

Received: October 28, 2011

Published: December 20, 2011

obtained increased to  $\sim 30$  mg. We also synthesized crystals containing the  $\{U_1CU_{28}CU_{40R}\}$  cluster in the absence of NaCl and obtained a similar yield of crystals, but their quality, as shown by X-ray diffraction, was inferior.

The synthesis of  $\{U_1CU_{28}CU_{40R}\}$  crystals was readily repeatable using a combination of tetraethylammonium hydroxide and one organic acid (malonic acid, 2-picolinic acid, citric acid, or DL-tartaric acid) to maintain the solution pH. Crystals containing  $\{U_1CU_{28}CU_{40R}\}$  were obtained from solutions with pH values in the range 9.7–11.2. The yield and quality of the crystals was not dependent on the organic acid used in the synthesis.

**2.2. Chemical Analysis.** Crystals of  $\{U_1CU_{28}CU_{40R}\}$  were isolated from their mother solution, rinsed with water, and mounted on a glass slide using double-sided tape. Laser ablation–inductively coupled plasma–mass spectrometry (LA-ICP-MS) analyses were performed on eight crystals using a ThermoFinnigan high-resolution magnetic sector Element2 ICP-MS instrument coupled to a UP213 Nd:YAG laser ablation system (New Wave Research). Individual analyses consisted of a 60 s measurement of background ion signals followed by a 60 s interval for measurement of ion signals ( $^{23}Na$ ,  $^{39}K$ ,  $^{235}U$ , and  $^{238}U$ ) subsequent to the start of ablation. Each analysis represented a total of 70 scans with a sample (dwell) time of 0.01 s and 20 samples per isotope ion signal. Analyses were conducted in medium mass resolution mode (resolution = mass/peak width  $\approx 4000$ ) to eliminate possible spectral interferences. The ablated particles were transported from the ablation cell to the ICP-MS instrument using He carrier gas at a flow rate of 1 L/min. Crystals were ablated using a laser spot size of 15  $\mu m$ , a repetition rate of 4 Hz, and 65% power output, corresponding to an energy density of 5 J/cm<sup>2</sup>.

The analysis confirmed the presence of both K and Na in  $\{U_1CU_{28}CU_{40R}\}$ . On the basis of 69 U atoms per  $\{U_1CU_{28}CU_{40R}\}$  cluster, as indicated by the crystal structure analysis, the numbers of K and Na atoms ranged from 32.7 to 38.2 [average = 36.3(8)] and 1.9 to 2.3 [average = 2.1(0.1)], respectively. The spectrum and analyses are provided in the Supporting Information.

**2.3. X-ray Crystallography.** Crystals were isolated from their mother solutions as soon as they had grown large enough for single-crystal X-ray diffraction studies. A suitable crystal was mounted on a cryoloop in oil and cooled by a flow of N<sub>2</sub> gas at a temperature of 100 K. Data were collected using a Bruker APEX II diffractometer equipped with graphite-monochromatized Mo K $\alpha$  radiation provided by a conventional X-ray source. A sphere of data was collected for the crystal using frame widths of 0.3° in  $\omega$ . Data were corrected for Lorentz, polarization, and background effects using the Bruker APEX II software, and an empirical correction for absorption was done using SADABS. Solution and refinement of the structure was done with the SHELXTL suite of software programs.<sup>30</sup> The final refinement included positional parameters for all atoms, anisotropic displacement parameters for U atoms, either anisotropic or isotropic displacement parameters for K atoms, and isotropic displacement parameters for all remaining atoms. H atoms were not located. There are eight symmetrically unique K sites in the structure; the occupancies of three of these were refined below full occupancy and presumably contained Na or vacancies.

The oxidation state of U(VI) in the structure was verified by a bond-valence analysis.<sup>31</sup> O atoms were assigned as O, OH, H<sub>2</sub>O, or peroxy ligands on the basis of bond-valence sums and, in the case of peroxy ligands, O–O bond lengths.

**2.4. Small-Angle X-ray Scattering.** SAXS data were collected using a Bruker Nanostar system equipped with a Cu microfocus source, Montel multilayer optics, and a HiSTAR multiwire detector. Data were collected using a sample-to-detector distance of 26.3 cm with the sample chamber under vacuum.

Crystals for analysis by SAXS were isolated from their mother solution by vacuum filtration. The crystals were rinsed with water, and visually clean crystals were harvested from the filter membrane and dissolved in ultrapure water. The resulting solutions were placed in 0.5 mm diameter glass capillaries, and the ends of each capillary were sealed using wax. Water was placed in an identical capillary for background measurements.

Following preparation of the synthesis reaction, aliquots of the solution were collected at various times for collection of SAXS data. These solutions were placed in glass capillaries, and SAXS data were collected as described above. The uranium content of these SAXS solutions was 0.77 M.

**2.5. Electrospray Ionization Mass Spectrometry.** Two groups of specimens were prepared for ESI-MS analysis. The first of these was prepared by dissolving crystals in ultrapure water. Crystals were removed from the glass vial in which they had grown and vacuum-filtered using a Whatman 1 filter membrane. The sample was then rinsed with 10 mL of ultrapure water, and crystals were hand-picked from the membrane. These crystals were dissolved in 50  $\mu L$  of ultrapure water, and the solution was diluted 10-fold using ultrapure water.

The second group of specimens consisted of samples of the reaction solution collected over time prior to formation of crystals of  $\{U_1CU_{28}CU_{40R}\}$ . For each sample, 500  $\mu L$  of the reaction solution was filtered using a Millex PTFE syringe filter with a pore size of 0.2  $\mu m$ . The filtrate was centrifuged in a 3 kDa Amicon centrifugal filter, rinsed with 400  $\mu L$  of water, and centrifuged three times. The solution was then diluted 1000-fold using ultrapure water. ESI-MS spectra were collected immediately following sample preparation. We estimate that the solutions measured contained 50–100 ppm U.

ESI-MS spectra<sup>32</sup> were collected in negative-ion mode using a Bruker micrOTOF-Q II high-resolution quadrupole time-of-flight (Q-TOF) spectrometer (3600 V capillary voltage, 0.8 bar nebulizer gas, 4 L/min dry gas, 180 °C dry gas temperature). The samples were introduced by direct infusion at 7  $\mu L$ /min and scanned over the range  $m/z$  500–5000 with data averaged over 5 min. The data were deconvoluted using MaxEnt software.

**2.6. Spectroscopic Characterization.** IR spectra were collected for both single crystals of  $\{U_1CU_{28}CU_{40R}\}$  and their thermogravimetric analysis (TGA) residue using a SensIR technology IlluminatIR FT-IR microspectrometer. A single crystal (or powder of TGA residue) was placed on a glass slide. The spectra were collected from 650 to 4000 cm<sup>-1</sup> with a beam aperture of 100  $\mu m$  using a diamond attenuated total reflection objective. The spectra collected for crystals readily confirmed the presence of uranyl ions and NO<sub>3</sub><sup>-</sup> and H<sub>2</sub>O groups. Uranyl ion stretches occurred at  $\sim 850$  cm<sup>-1</sup>, NO<sub>3</sub><sup>-</sup> modes at  $\sim 1320$  cm<sup>-1</sup>, and a H<sub>2</sub>O bending mode at  $\sim 1680$  cm<sup>-1</sup>; O–H bonds were indicated by the broad envelope from about 2600 to 3600 cm<sup>-1</sup>. The spectrum of TGA residue confirmed that H<sub>2</sub>O, OH<sup>-</sup>, and NO<sub>3</sub><sup>-</sup> groups were lost during the TGA measurement. The IR spectra are given in the Supporting Information.

A UV–vis spectrum was collected for a single crystal of  $\{U_1CU_{28}CU_{40R}\}$  using a Craic Technologies microspectrophotometer. The crystal was placed on a quartz slide under mineral oil, and the data were collected from 250 to 1400 nm. The spectrum is shown in the Supporting Information.

**2.7. Thermogravimetric Analysis.** TGA measurements were conducted with a Netzsch TG209 F1 Iris thermal analyzer using 11.93 mg of  $\{U_1CU_{28}CU_{40R}\}$  crystals in an Al crucible. The sample was heated from 20 to 600 °C at a rate of 5 °C/min under flowing nitrogen gas. The total weight loss by 600 °C was 25%. The TGA data are provided in the Supporting Information.

### 3. RESULTS

**3.1. Structure of  $\{U_1CU_{28}CU_{40R}\}$ .** The structure study revealed that  $\{U_1CU_{28}CU_{40R}\}$  is an extraordinarily complex cluster that is built from uranyl polyhedra and NO<sub>3</sub> triangles (Figures 1 and 2). One partially occupied U site is located at the center of the cluster, 28 are located in a shell ranging from 6.84 to 7.06 Å from the cluster center, and 40 are arranged in a shell ranging from 12.33 to 12.48 Å from the cluster center.

We first consider the U(VI) cations in the small shell, ranging from 6.84 to 7.06 Å from the cluster center. Each occurs as a typical (UO<sub>2</sub>)<sup>2+</sup> dioxo cation. Each uranyl ion is coordinated by six O atoms arranged at the equatorial vertices

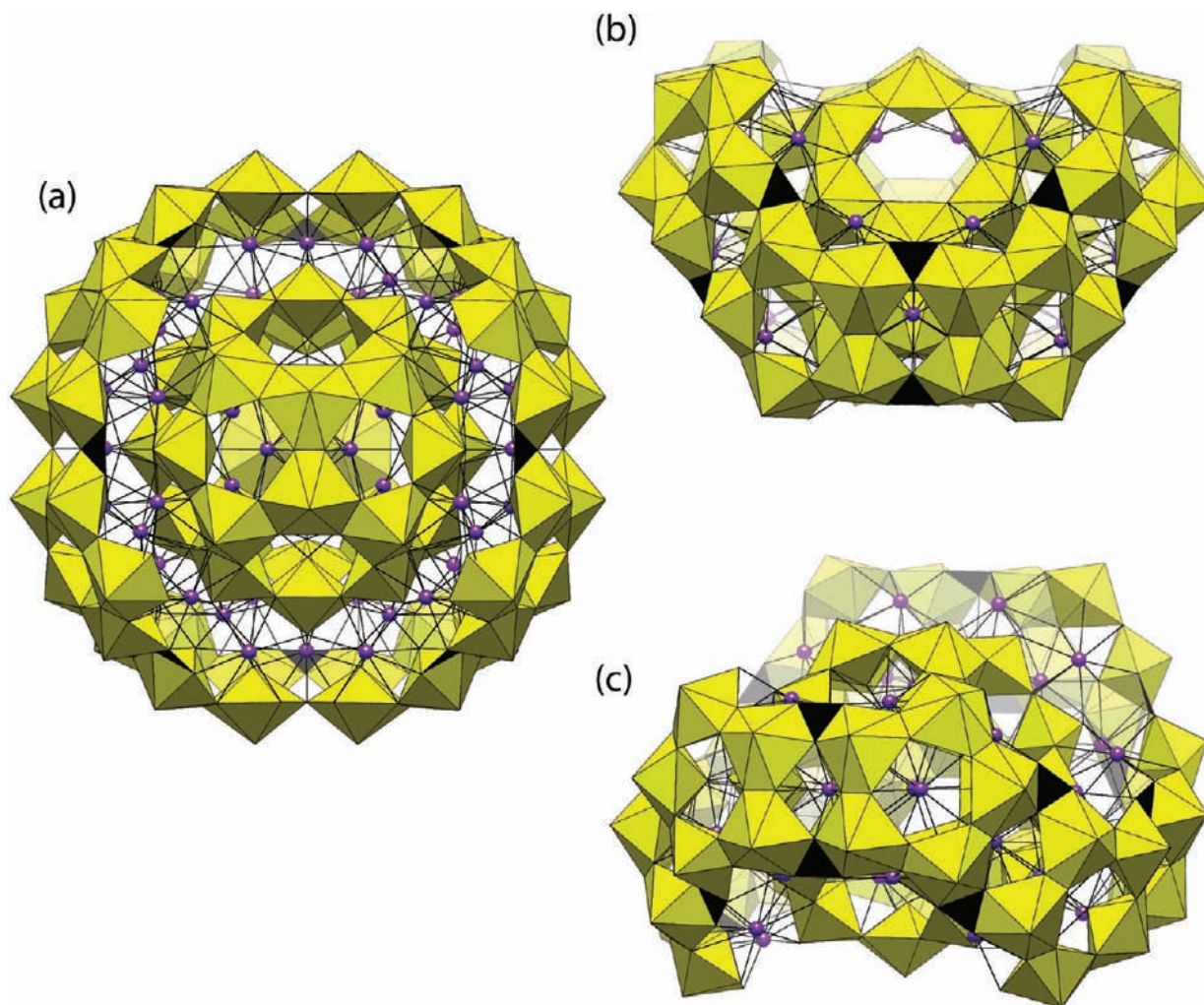


**Figure 1.** Mixed polyhedral and ball-and-stick representations of  $\{U_1C U_{28} C U_{40R}\}$ . The central  $U_{28}$  cage cluster is surrounded by the  $U_{40R}$  shell, and these are linked together through  $K-O$  bonds. (a) View of  $\{U_1C U_{28} C U_{40R}\}$  along the  $\bar{4}$  rotational axis. (b) Side view of  $\{U_1C U_{28} C U_{40R}\}$  showing the boatlike shape of the  $U_{40R}$  shell with the  $U_{28}$  cage cluster nestled within it. (c) View of  $\{U_1C U_{28} C U_{40R}\}$  oriented to demonstrate the correspondence of five-membered rings of uranyl bipyramids in the  $U_{28}$  and  $U_{40R}$  shells. Uranyl polyhedra are shown in yellow, nitrate triangles in black, and  $K^+$  cations as purple balls.

of hexagonal bipyramids. Each bipyramid shares three of its equatorial edges with adjacent uranyl bipyramids, resulting in a cage cluster consisting of 28 uranyl hexagonal bipyramids, designated as  $U_{28}$  (Figure 2 b,c).

The uranyl ion of one symmetrically distinct site is coordinated by three peroxo ligands that are bidentate to the uranyl ion, with peroxo  $O-O$  bond lengths in the range  $1.41(4)-1.54(4)$  Å. The  $O_{eq}-O_{eq}$  interatomic distances of shared polyhedral edges of the remaining uranyl ions in  $U_{28}$  fall into two groups. One-third of them are in the range  $1.41(4)-1.54(4)$  Å and correspond to peroxo ligands. The remaining two-thirds fall in the range  $1.88(4)-2.05(4)$  Å, which is too long to correspond to peroxo ligands and too short to be pairs of hydroxyl groups. Rather, these values cluster around the average of two peroxo  $O-O$  bond lengths of  $\sim 1.5$  Å and one  $OH-OH$  separation of  $\sim 2.8$  Å. We therefore conclude that these uranyl ions are either coordinated by two peroxo groups as well as two hydroxyl groups in a cis arrangement, as has been found in a wide range of clusters built from uranyl polyhedra, or by three peroxo groups, which is also common. In this case, there are two or more versions of the cluster that are averaged in the X-ray diffraction data, giving the apparent  $O_{eq}-O_{eq}$

separations. The  $U_{28}$  cluster thus contains four uranyl ions that are coordinated by three peroxo groups, with the remaining 24 coordinated by either two or three peroxo groups each. The composition of the uranyl polyhedral component of the cluster is approximately  $[(UO_2)_{28}(O_2)_{34}(OH)_{16}]^{28-}$ .

The  $U_{28}$  cluster is topologically identical to that which we reported earlier.<sup>26</sup> Its graphical representation is shown in Figure 2d. Each vertex in the graph corresponds to a  $U^{6+}$  cation in  $U_{28}$ , and lines connecting vertices denote polyhedral edges that are shared between the corresponding uranyl polyhedra. The  $U_{28}$  cluster adopts a fullerene topology consisting of 12 pentagons and four hexagons. There are 16 cation sites located within the cage that contain  $K^+$  (and possibly  $Na^+$ ), with one positioned inside each of the pentagons and hexagons of the topology. Nyman<sup>33</sup> examined the  $U_{28}$  cluster with composition  $[(UO_2)(O_2)_{1.5}]_{28}$  and inserted  $Rb^+$ ,  $K^+$ ,  $Cs^+$ , and even  $Nb(O_2)_4$  and  $Ta(O_2)_4$  inside the cage.

We next consider the 40  $U(VI)$  cations that are located in the shell ranging from 12.33 to 12.48 Å from the cluster center (Figure 2e,f). Each of the  $U(VI)$  cations are present as a typical  $(UO_2)^{2+}$  uranyl ion. Each uranyl ion is coordinated by two peroxo ligands that are bidentate to the uranyl ion, and each

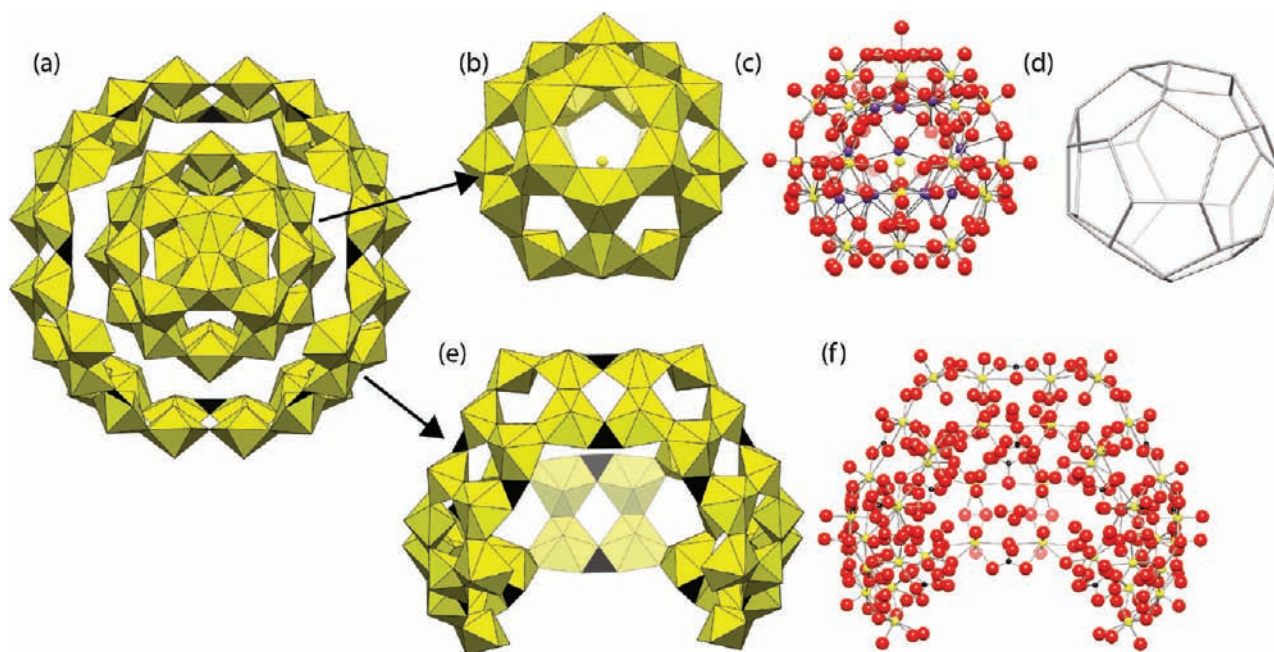


**Figure 2.** Polyhedral and ball-and-stick representations of the  $\{U_1C U_{28}C U_{40R}\}$  cluster emphasizing (b–d) the  $U_{28}$  cage cluster with a U atom at the center and (e, f) the  $U_{40R}$  shell. A graphical representation of the  $U_{28}$  cage cluster is shown in (d), in which each vertex of the graph corresponds to a U cation in the cluster. Vertices in the graph are connected where their corresponding uranyl polyhedra share equatorial edges.

peroxo ligand is shared between two uranyl ions, resulting in eight five-membered rings of bipyramids. Nitrate groups that are bidentate to the uranyl ion contribute the remaining two equatorial vertices of four of the uranyl hexagonal bipyramids in any five-membered ring (Figure 2e). For one uranyl bipyramid of each five-membered ring, the coordination environment about the uranyl ion is completed by two  $H_2O$  groups located at equatorial vertices on the same side of the bipyramid.

Each five-membered ring of uranyl bipyramids is linked to two others in a novel fashion (Figure 2e). Two adjacent bipyramids share single vertices with two bipyramids of the next ring, forming four-membered rings of bipyramids. Two nitrate groups are located within this ring of bipyramids in such a way that they coordinate two uranyl ions, both in bidentate configurations.

The 40 uranyl bipyramids and 16 nitrate groups that occur in the larger shell link to form a boat-shaped ring designated as  $U_{40R}$ , as shown in Figures 1 and 2. The composition of the uranyl polyhedral and nitrate shell is  $[(UO_2)_{40}(O_2)_{40}(H_2O)_{16}(NO_3)_{16}]^{16-}$ .

The  $\{U_1C U_{28}C U_{40R}\}$  cluster contains a single U site at its center. Refinement of the occupancy of this site, which is located on a special position with symmetry  $\bar{4}2m$ , indicates that it is  $\sim 50\%$  occupied by U. This is too much electron density to be accounted for by any other constituent in the synthesis reaction. However, the coordination environment about this site is disordered, with numerous peaks in the difference Fourier map at plausible distances from the U cation. We note that the site symmetry is incompatible with the presence of an ordered uranyl ion or a bipyramidal coordination geometry. We are therefore unable to identify the oxidation state or coordination environment of this site, but the synthesis conditions and dominance of U(VI) in the cluster overall are consistent with the central site also being occupied by U(VI).

When only the uranyl and nitrate polyhedra are considered, the overall  $\{U_1C U_{28}C U_{40R}\}$  cluster consists of three shells: the central U position, the  $U_{28}$  fullerene-topology closed cluster as the second shell, and the uranyl peroxo nitrate  $U_{40R}$  ring as the third shell.

Fourteen  $K^+/Na^+$  cations are located within the  $U_{28}$  cage cluster (Figure 2c), distributed over 16 partially occupied sites, and may provide linkages to the central U site. More significant to the overall cluster assembly and appearance are the 40  $K^+$  cations that are located between the second ( $U_{28}$ ) and third ( $U_{40R}$ ) shells (Figure 1). Eight of these are located inside the eight five-membered rings of uranyl hexagonal bipyramids of the  $U_{40R}$  shell in such a way that they are bonded to the O atoms of all five of the uranyl ions in the ring. The five-membered rings of hexagonal bipyramids in the  $U_{40R}$  shell are in direct correspondence with those of the  $U_{28}$  shell. The eight  $K^+$  cations are coordinated by one O of each of the five peroxo groups of the five-membered ring in  $U_{28}$ , and thus each  $K^+$  is 10-coordinated by O atoms, five from either shell. The remainder of the  $K^+$  cations are also located between the  $U_{28}$  and  $U_{40R}$  shells, bonded to O atoms of uranyl ions and O atoms of peroxo ligands of each shell.

The unusual configuration of the  $U_{40R}$  shell appears to have been templated by the  $U_{28}$  cluster. Specifically, each five-membered ring of hexagonal bipyramids in  $U_{40R}$  is directly above a corresponding five-membered ring of bipyramids in the  $U_{28}$  shell, and these rings are linked through the  $K^+$  cations between them. The locations of these rings of bipyramids in  $U_{40R}$  are guided by the location of pentagons in the fullerene topology of  $U_{28}$ .

**3.2. Composition of  $\{U_1C U_{28}C U_{40R}\}$ .** The crystal structure analysis of  $\{U_1C U_{28}C U_{40R}\}$  provided the chemical formula  $(K,Na)_{44}[(UO_2)_{68}(O_2)_{74}(OH)_{16}(NO_3)_{16}(H_2O)_{16}](H_2O)_n$ , neglecting the partially occupied U site at the center of the cluster.  $K^+$  is dominant in the partially occupied sites within

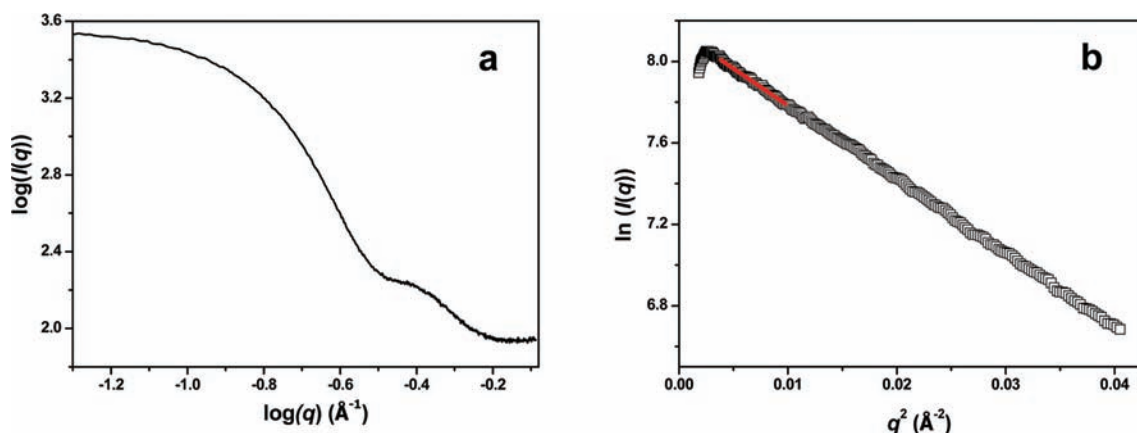


Figure 3. Log–log and Guinier plots of SAXS data collected for an aqueous solution created by dissolving crystals of  $\{U_1CU_{28}CU_{40R}\}$ .

the  $U_{28}$  shell, although  $Na^+$  substitution is possible and was indicated by the chemical analysis. The chemical analyses confirmed the  $K^+$  content and suggest a  $Na^+$  content of  $\sim 2$   $Na^+$  per formula unit. The TGA data indicated that  $n \approx 155$ .

**3.3. SAXS and ESI-MS Studies of Dissolved  $\{U_1CU_{28}CU_{40R}\}$ .** Water in which crystals of  $\{U_1CU_{28}CU_{40R}\}$  had been dissolved scattered X-rays in the low- $q$  region (Figure 3). The radius of gyration,  $R_g$ , of the macroions in solution was determined using Guinier analysis of the low- $q$  data.  $R_g$  is the root-mean-square average of the mass-weighted distances of all subvolumes in a particle from the center of mass of the particle.<sup>34</sup> The value of  $R_g$  derived from the data was 10.44 Å, which compares well with that derived from the crystallographic data using the CRY SOL<sup>35</sup> program (10.45 Å). The SAXS data demonstrated that clusters of  $\{U_1CU_{28}CU_{40R}\}$  dissolved in ultrapure water remained intact.

The  $U_{28}$  inner shell, including the  $K^+$  and  $Na^+$  cations enclosed in the cage cluster, has a mass of  $\sim 9100$  Da. The mass of the entire  $\{U_1CU_{28}CU_{40R}\}$  cluster, including the  $K^+$  and  $Na^+$  cations, is  $\sim 24$  kDa. Deconvolution of the ESI-MS data (Figure 4) collected for a solution derived by dissolving crystals of  $\{U_1CU_{28}CU_{40R}\}$  in water gave masses in the range 21815.44–23453.08 Da, with an average mass of 22605 Da. The  $\{U_1CU_{28}CU_{40R}\}$  cluster remained intact during our mass spectrometry measurements.

**3.4. Time-Resolved ESI-MS and SAXS Studies.** We used ESI-MS and SAXS studies to monitor the self-assembly of  $\{U_1CU_{28}CU_{40R}\}$  in solution prior to crystallization. We also crystallized the  $U_{28}$  cluster we reported earlier for comparison to  $\{U_1CU_{28}CU_{40R}\}$ . Time-resolved ESI-MS data (Figure 4) showed that the average mass of the species in solution after 1 h was similar to that of the  $U_{28}$  cluster ( $\sim 10$  kDa). Much later, after  $\sim 15$  days, the data indicated the presence of two dominant species in solution, with masses of approximately 10 and 22 kDa. We interpret this to indicate that at this point the solution contained both  $U_{28}$  and the larger  $\{U_1CU_{28}CU_{40R}\}$  cluster.

The time-resolved SAXS data provided additional insight into the  $\{U_1CU_{28}CU_{40R}\}$  self-assembly process (Figure 5).  $R_g$  values were calculated using Guinier analysis for each scattering pattern (see the Supporting Information). As shown in Figure 6,  $R_g$  for the 1 h samples was  $\sim 6.57$  Å, which is similar to the value of 6.87 Å for the  $U_{28}$  cluster calculated from atomic coordinates of the crystal structure using the CRY SOL method. With increasing time,  $R_g$  increased. After  $\sim 1$  month, crystals containing  $\{U_1CU_{28}CU_{40R}\}$  formed, and the measured  $R_g$  was

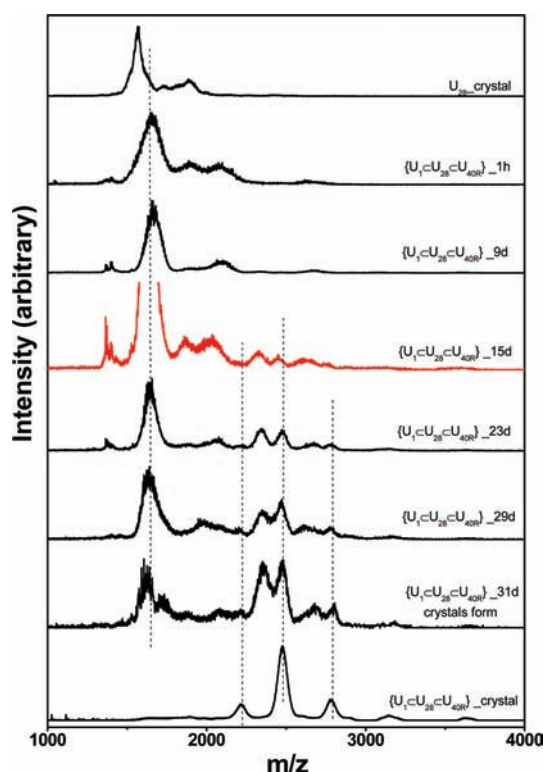


Figure 4. ESI-MS data for samples made using different-time-aged reaction solutions of  $\{U_1CU_{28}CU_{40R}\}$  clusters and samples made using crystals of  $\{U_1CU_{28}CU_{40R}\}$  and  $U_{28}$  clusters.

10.36 Å, which is close to that of  $\{U_1CU_{28}CU_{40R}\}$  dissolved in ultrapure water.

We calculated the distance pair distribution function (PDF),  $p(r)$ , using an indirect Fourier transform of the primary SAXS data;<sup>36</sup>  $p(r)$  is the probability of finding a vector length in the molecule having a value equal to  $r$ ; this probability becomes zero at the maximum vector length,  $r_{max}$ <sup>34</sup> which equals the largest linear dimension in a particle. The time evolution of the  $p(r)$  plots is shown in the Supporting Information, and that of  $r_{max}$  is given in Figure 7. In the short-duration experiments,  $r_{max} \approx 18$  Å, consistent with the maximum diameter between the outer edges of bounding O atoms of  $U_{28}$ . The measured  $r_{max}$  increased with time. After the solution had been aged for 1 month,  $r_{max}$  reached 27 Å, a value similar to the maximum diameter

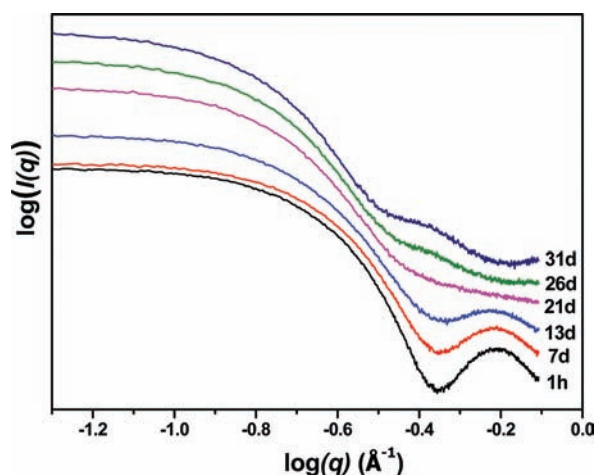


Figure 5. Selected SAXS log–log plots for the different-time-aged reaction solutions of  $\{U_1C U_{28}C U_{40R}\}$  clusters.

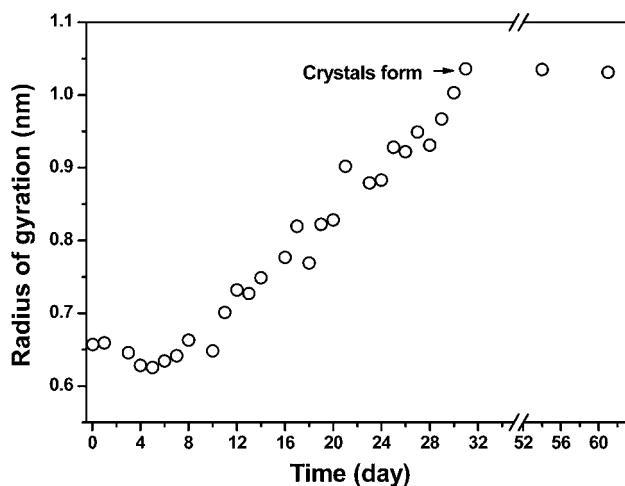


Figure 6. Evolution of the radius of gyration ( $R_g$ ) of clusters in the solution with increasing aging time.  $R_g$  values were calculated from the SAXS data using Guinier analysis.

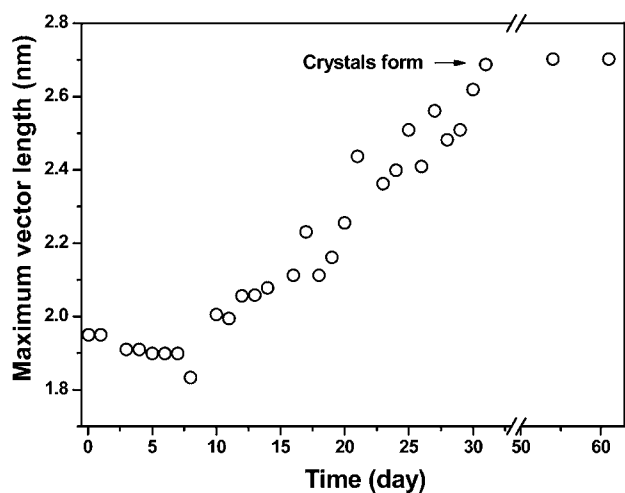


Figure 7. Evolution of the maximum vector length ( $r_{max}$ ) of the clusters in the solution with increasing aging time. Values of  $r$  were calculated from the SAXS data by Moore analysis.

measured between the outer edges of bounding O atoms of  $U_{40R-z}$

#### 4. DISCUSSION

We have presented the first time-resolved study of the self-assembly of a nanoscale uranyl peroxide cluster. The cluster consists of multiple shells of uranyl polyhedra, with the inner  $U_{28}$  fullerene-topology shell clearly templating the outer  $U_{40R}$  shell by connections through K cations.

The  $U_{28}$  clusters rapidly assemble in solution once the reactants have been mixed under ambient conditions. They are demonstrably present within 1 h of synthesis, which is the shortest time we needed to collect SAXS or ESI-MS data. The  $U_{28}$  cluster appears to persist in solution for several days without significant change. After  $\sim 10$  days, the average size of clusters in solution begins to increase, and growth continues to  $\sim 30$  days, at which time crystals containing  $\{U_1C U_{28}C U_{40R}\}$  form. Cluster growth may be triggered by evaporation of the solution, with the concomitant increase in the concentration of uranyl ions in solution.

$\{U_1C U_{28}C U_{40R}\}$  is the first core–shell cluster reported in the uranyl peroxo system. The scarcity of such a configuration presumably relates to the orientations of the uranyl ions within cage clusters. All single-shell cage clusters built from uranyl peroxo polyhedra reported to date exhibit polyhedral linkages through equatorial edges, with the uranyl ions extending perpendicular to the cage wall. The strong triple bond within the uranyl ion makes its O atoms relatively unreactive, and direct linkages of uranyl ions through these O atoms are rare. In  $\{U_1C U_{28}C U_{40R}\}$ , it is the  $K^+$  cations that bridge the  $U_{28}$  core and  $U_{40R}$  shell, as these ions readily coordinate the O atoms of uranyl ions.

#### ■ ASSOCIATED CONTENT

##### Supporting Information

LA-ICP-MS, UV–vis, IR, TGA, and SAXS data; crystallographic data, atomic coordinates, and geometrical parameters; and a CIF file. This material is available free of charge via the Internet at <http://pubs.acs.org>.

#### ■ AUTHOR INFORMATION

##### Corresponding Author

[pburns@nd.edu](mailto:pburns@nd.edu)

#### ■ ACKNOWLEDGMENTS

This material is based upon work supported as part of the Materials Science of Actinides Center, an Energy Frontier Research Center funded by the U.S. Department of Energy, Office of Science, Office of Basic Energy Sciences, under Award DE-SC0001089. The electrospray data are based upon work supported by the National Science Foundation under CHE-0741793.

#### ■ REFERENCES

- (1) Pope, M. T.; Muller, A. *Angew. Chem., Int. Ed. Engl.* **1991**, *30*, 34–48.
- (2) Muller, A.; Peters, F.; Pope, M. T.; Gatteschi, D. *Chem. Rev.* **1998**, *98*, 239–271.
- (3) Liu, T. B.; Imber, B.; Diemann, E.; Liu, G.; Cokleski, K.; Li, H. L.; Chen, Z. Q.; Muller, A. *J. Am. Chem. Soc.* **2006**, *128*, 15914–15920.
- (4) Burns, P. C. *Mineral. Mag.* **2011**, *75*, 1–25.
- (5) Long, D. L.; Tsunashima, R.; Cronin, L. *Angew. Chem., Int. Ed.* **2010**, *49*, 1736–1758.
- (6) Muller, A.; Roy, S. *Coord. Chem. Rev.* **2003**, *245*, 153–166.
- (7) Miras, H. N.; Cooper, G. J. T.; Long, D. L.; Bogge, H.; Muller, A.; Streb, C.; Cronin, L. *Science* **2010**, *327*, 72–74.

- (8) Morss, L. R.; Edelstein, N. M.; Fuger, J.; Katz, J. J. *The Chemistry of the Actinide and Transactinide Elements*; Springer: Dordrecht, The Netherlands, 2006.
- (9) Nocton, G.; Burdet, F.; Pecaut, J.; Mazzanti, M. *Angew. Chem., Int. Ed.* **2007**, *46*, 7574–7578.
- (10) Nocton, G.; Pecaut, J.; Filinchuk, Y.; Mazzanti, M. *Chem. Commun.* **2010**, *46*, 2757–2759.
- (11) Nocton, G.; Pecaut, J.; Mazzanti, M. *Angew. Chem., Int. Ed.* **2008**, *47*, 3040–3042.
- (12) Biswas, B.; Mougél, V.; Pecaut, J.; Mazzanti, M. *Angew. Chem., Int. Ed.* **2011**, *50*, 5744–5747.
- (13) Duval, P. B.; Burns, C. J.; Clark, D. L.; Morris, D. E.; Scott, B. L.; Thompson, J. D.; Werkema, E. L.; Jia, L.; Andersen, R. A. *Angew. Chem., Int. Ed.* **2001**, *40*, 3358–3361.
- (14) Soderholm, L.; Almond, P. M.; Skanthakumar, S.; Wilson, R. E.; Burns, P. C. *Angew. Chem., Int. Ed.* **2008**, *47*, 298–302.
- (15) Unruh, D. K.; Ling, J.; Qiu, J.; Pressprich, L.; Baranay, M.; Ward, M.; Burns, P. C. *Inorg. Chem.* **2011**, *50*, 5509–5516.
- (16) Sigmon, G. E.; Burns, P. C. *J. Am. Chem. Soc.* **2011**, *133*, 9137–9139.
- (17) Ling, J.; Qiu, J.; Szymanowski, J. E. S.; Burns, P. C. *Chem.—Eur. J.* **2011**, *17*, 2571–2574.
- (18) Ling, J.; Wallace, C. M.; Szymanowski, J. E. S.; Burns, P. C. *Angew. Chem., Int. Ed.* **2010**, *49*, 7271–7273.
- (19) Ling, J.; Qiu, J.; Sigmon, G. E.; Ward, M.; Szymanowski, J. E. S.; Burns, P. C. *J. Am. Chem. Soc.* **2010**, *132*, 13395–13402.
- (20) Burns, P. C. *C. R. Chim.* **2010**, *13*, 737–746.
- (21) Unruh, D. K.; Burtner, A.; Pressprich, L.; Sigmon, G. E.; Burns, P. C. *Dalton Trans* **2010**, *39*, 5807–5813.
- (22) Sigmon, G. E.; Weaver, B.; Kubatko, K.-A.; Burns, P. C. *Inorg. Chem.* **2009**, *48*, 10907–10909.
- (23) Sigmon, G. E.; Unruh, D. K.; Ling, J.; Weaver, B.; Ward, M.; Pressprich, L.; Simonetti, A.; Burns, P. C. *Angew. Chem., Int. Ed.* **2009**, *48*, 2737–2740.
- (24) Sigmon, G. E.; Ling, J.; Unruh, D. K.; Moore-Shay, L.; Ward, M.; Weaver, B.; Burns, P. C. *J. Am. Chem. Soc.* **2009**, *131*, 16648–16649.
- (25) Forbes, T. Z.; McAlpin, J. G.; Murphy, R.; Burns, P. C. *Angew. Chem., Int. Ed.* **2008**, *47*, 2824–2827.
- (26) Burns, P. C.; Kubatko, K.-A.; Sigmon, G.; Fryer, B. J.; Gagnon, J. E.; Antonio, M. R.; Soderholm, L. *Angew. Chem., Int. Ed.* **2005**, *44*, 2135–2139.
- (27) Miro, P.; Pierrefixe, S.; Gicquel, M.; Gil, A.; Bo, C. *J. Am. Chem. Soc.* **2010**, *132*, 17787–17794.
- (28) Vlaisavljevich, B.; Gagliardi, L.; Burns, P. C. *J. Am. Chem. Soc.* **2010**, *132*, 14503–14508.
- (29) Fang, X.; Koegerler, P.; Furukawa, Y.; Speldrich, M.; Luban, M. *Angew. Chem., Int. Ed.* **2011**, *50*, 5212–5216.
- (30) Sheldrick, G. M. *SHELXTL*; Bruker AXS, Inc.: Madison, WI, 2008.
- (31) Burns, P. C.; Ewing, R. C.; Hawthorne, F. C. *Can. Mineral.* **1997**, *35*, 1551–1570.
- (32) Fenn, J. B.; Mann, M.; Meng, C. K.; Wong, S. F.; Whitehouse, C. M. *Science* **1989**, *246*, 64–71.
- (33) Nyman, M.; Rodriguez, M. A.; Alam, T. M. *Eur. J. Inorg. Chem.* **2011**, 2197–2205.
- (34) Feigin, L. A.; Svergun, D. I. *Structure Analysis by Small-Angle X-Ray and Neutron Scattering*; Plenum Press: New York, 1987.
- (35) Svergun, D.; Barberato, C.; Koch, M. H. J. *J. Appl. Crystallogr.* **1995**, *28*, 768–773.
- (36) Moore, P. B. *J. Appl. Crystallogr.* **1980**, *13*, 168–175.